PAPER

Fluorine doped SnO_2 (FTO) nanobelts: some data on electronic parameters

IOP Publishing Journal of Physics D: Applied Physics
J. Phys. D: Appl. Phys. **47** (2014) 045301 (6pp) doi:10.1088/0022-3727/47/4/045301

Fluorine doped SnO_2 (FTO) nanobelts: some data on electronic parameters

Cleber A Amorim[1], Cleocir J Dalmaschio[2], Edson R Leite[2] and Adenilson J Chiquito[1]

[1] NanoLab, Departamento de Física, Universidade Federal de São Carlos–UFSCar, Rodovia Washington Luiz, Km 235 Monjolinho, CP 676, CEP 13565-905, São Carlos, São Paulo, Brazil
[2] LIEC, Departamento de Química, Universidade Federal de São Carlos–UFSCar, Rodovia Washington Luiz, Km 235 Monjolinho, CEP 13565-905, São Carlos, São Paulo, Brazil

E-mail: murinm81@gmail.com

Received 19 August 2013, revised 30 October 2013
Accepted for publication 12 November 2013
Published 20 December 2013

Abstract

Fluorine doped SnO_2 (FTO) nanobelts were synthesized and their transport properties, such as conduction mechanism, mobility, carrier density and density of states (DOS) were investigated. Variable range hopping was observed as the dominant mechanism in a large range of temperature (40–260 K). Through these data we estimated the localization length and hopping distance at 300 K of FTO nanobelts exhibiting a three-dimensional character for carrier transport. The carrier mobility was calculated to be 48 $cm^2\ V^{-1}\ s^{-1}$ for samples with carrier density of $2 \times 10^{18}\ cm^{-3}$. Taking into account the parameters obtained from temperature-dependent resistivity and the above data, the characteristic DOS at Fermi level in our samples was found.

Keywords: field effect transistor, electronic transport, variable range hopping, electron mobility, fluorine doped tin oxide

(Some figures may appear in colour only in the online journal)

1. Introduction

Nanostructured materials have been a fundamental basis for technological advances in miniaturization and development of optoelectronic devices: decreasing material's density and increasing its strength, is fundamental for basic science. These materials are technologically imperative since the performance of such devices is critically dependent on the dimension or the surface-to-volume ratio of the material [1] with particular attention to transparent conductive oxides (TCOs). These materials are a unique group that offer both high optical transmissivity in the visible range and low electrical resistivity. TCO materials such as SnO_2, In_2O_3 and ZnO [2–4] have been widely studied in the form of nanowires, nanotubes and nanobelts. They also provide a useful basis to study some aspects of basic physics such as weak localization (quantum corrections to the classical conductivity) [5].

Some TCOs properties have attracted much attention such as those investigated by Lupan *et al*, in hydrogen single and multiple nanowire nanosensors based on ZnO [6]. In that work the authors showed an enhanced gas response and selectivity for the detection of hydrogen at room temperature compared to previously reported H_2 nanosensors. Additionally, the gas response was shown to depend on the Cd-doping, and to be significantly improved as compared to undoped ZnO. In the same way, ethanol gas sensing properties of SnO_2 nanobelts functionalized with Au were studied and an improvement in the responses of the nanobelts by approximately 100 times at 50 and 100 ppm C_2H_5OH with Au functionalized samples were observed [7]. Furthermore, Changhyun Jin *et al*, presented that SnO_2–ZnO coaxial nanowires have their photoluminescence properties enhanced after annealing process [8]. Also, new growth methods have been implemented for better understanding or performance of nanosctructured device. For instance, Lupan *et al*, showed a rapid fabrication technique for tin oxide nanowires with rutile structure synthesized by the hydrothermal method, allowing rapid and controlled growth of samples [9]. Additionally, transparent conducting nanobelts have also been used as the channel to field-effect transistors (FETs) and for detection of

different chemical species, transparent and flexible electronics, memories and integrated logic circuits [10–14].

Early studies on TCO nanostructures were focused on undoped samples in which electrons were supplied by deviation from stoichiometry (oxygen vacancies) or unintentional doping by impurities (uncontrolled) in the growth facility [15–18]. Undoped samples are usually characterized by low and unstable conductivity (accordingly to the surrounding atmosphere) [19]. Such issues, which are present even in thin films, can be controlled by doping with impurities such as Zn, Sb, In and F as shown in literature for both thin films and nanobelts [20–23].

As a matter of fact, Shanthi *et al* showed that 57 at% FTO films present excellent resistivity ($<10^{-3}\,\Omega\,\mathrm{cm}$) and high visible transparency (>88%) [24] when compared to ITO. More recently, a comparative study between ITO and FTO films proposed by Aouaj *et al*, presented that electrical resistivity was $8 \times 10^{4}\,\Omega\,\mathrm{cm}$ and $6 \times 10^{-4}\,\Omega\,\mathrm{cm}$ for ITO (6% of Sn) and FTO (2.5% of F), respectively [25]. In the same way, Bilgin *et al*, observed that electrical conductivity of fluorine doped SnO_2 films increased by two orders of magnitude up to 5% of dopant [26]. Likewise Wan *et al*, showed that films of antimony doped SnO_2 nanobelts have observed a much better response than that achieved in undoped ones [27]. Among the various alternatives the fluorine doped SnO_2 is also interesting because it shows high transparency and excellent conductivity as observed in thin film [28] samples. Therefore, fluorine doped SnO_2 may provide an inexpensive alternative to indium doped tin oxide (ITO) as transparent conducting oxide materials because they are synthesized by a simple and economical technique (vapour–solid (VS)) [29] and do not present unstable phases of SnO_2 (Sn_3O_4) [30]; additionally they present high crystallinity [26] and have similar transport parameters of ITO [25]. In this context, the electrical properties of fluorine doped SnO_2 (FTO) samples should be carefully studied to identify the compatibilities with ITO device applications.

Here we report some electrical data on FTO nanobelts. We successfully synthesized FTO nanobelts with controlled characteristics and developed a useful device with them. The underlying conduction mechanism was identified as the variable range hopping (VRH) process. Combining the parameters obtained from temperature-dependent with electrical data from FETs (with FTO nanobelts as active channels) we calculated the characteristic carrier mobility and density. Also, the density of states (DOS) of the samples was calculated in close agreement with values estimated from literature.

2. Sample structure and methods

The FTO nanobelts were synthesized by a carbothermal evaporation associated with the well known VS mechanism. In FTO synthesis the tin source is the SnO_2 (Aldrich, >325 mesh, purity >99.9%) which was mixed with graphite (Aldrich, >20 μm, purity >99 %) 95 : 5 in weight, respectively, by using a balls mill for 24 h. The obtained mixture was placed in a crucible and then it was placed at the centre of a horizontal tube furnace (Lindberg Blue M), where the temperature, gas flux and evaporation time were controlled in order to obtain the best conditions for the synthesis. Near to each tube extremity was placed an alumina boat with 0.5 g NH_4F, used as fluorine source. The tube atmosphere was controlled during all the synthesis procedure. From room temperature to 600 °C an inert atmosphere was used, keeping 100 SCCM N_2 flow. From 600 °C to the end of the synthesis time a controlled O_2 quantity was admitted in both tube extremities. The synthesis was carried out at 1200 °C for 2 h, using a 10 °C min^{-1} as heating rate. The white material collected after the synthesis was structurally and electrically characterized.

The material structure was analysed by x-ray diffraction (XRD) using a Rigaku diffractometer model DMAX 2500PC, with Cu–Kα radiation ($\lambda = 1.540\,56$ Å) at 40 kV and 150 mA. A scanning electron microscope (SEM) FEI INSPECT F50 equipped with an energy-dispersive x-ray spectrometer EDAX was used in microanalysis (EDX) and microstructure characterization. Single SnO_2 : F nanobelt devices were simply prepared by a conventional random dispersion technique and ohmic contacts were made by alloying small pieces of indium (~200 μm) into the belt + subtrate at 450 °C for 10 min in a tube furnace filled with an inert argon atmosphere. These devices were used to investigated the temperature dependence of resistivity.

Back-gated devices were prepared by conventional photolitography producing a FET structure. The transistor channel was produced by dropping a micrometre volume of an ethanol + FTO nanobelts solution onto a oxidized silicon substrate (where Au/Ni electrical contacts were previously prepared). Next, the devices were annealed at 450 °C for 20 min in a conventional tube furnace filled with argon. The transport measurements were carried out at different temperatures from 10 to 300 K using a closed cycle helium cryostat and at pressures lower than 5×10^{-6} mbar. Temperature-dependent resistivity was measured using standard low-frequency lock-in techniques ($f = 13$ Hz) with a Keithley 6221 as a current source. The current–voltage curves at different temperatures were obtained by using a Keithley 237 source meter unit.

3. Results and discussion

The as-grown fluorine doped SnO_2 samples were firstly studied by XRD. Figure 1(*a*) presents the diffraction pattern indexed as cassiterite (PDF # 41-1445). In order to compare the relative intensity (*hkl*) peaks from FTO samples with indexed cassiterite PDF, the intensity was analysed. The XRD pattern from the nanobelts present higher intensity in (1 0 1) than (1 1 0). The intensity relation I_{101}/I_{110} is inverted if compared with the PDF file mentioned above; we believe this inversion is associated with the directional and single crystalline character of nanobelts when supported in XRD sample holder. The material presents a preferred orientation (textured sample) as a consequence of morphological structure resulting in a change in the relative intensity compared with the indexed PDF. In order to check whether SnO_2 nanobelts were doped with

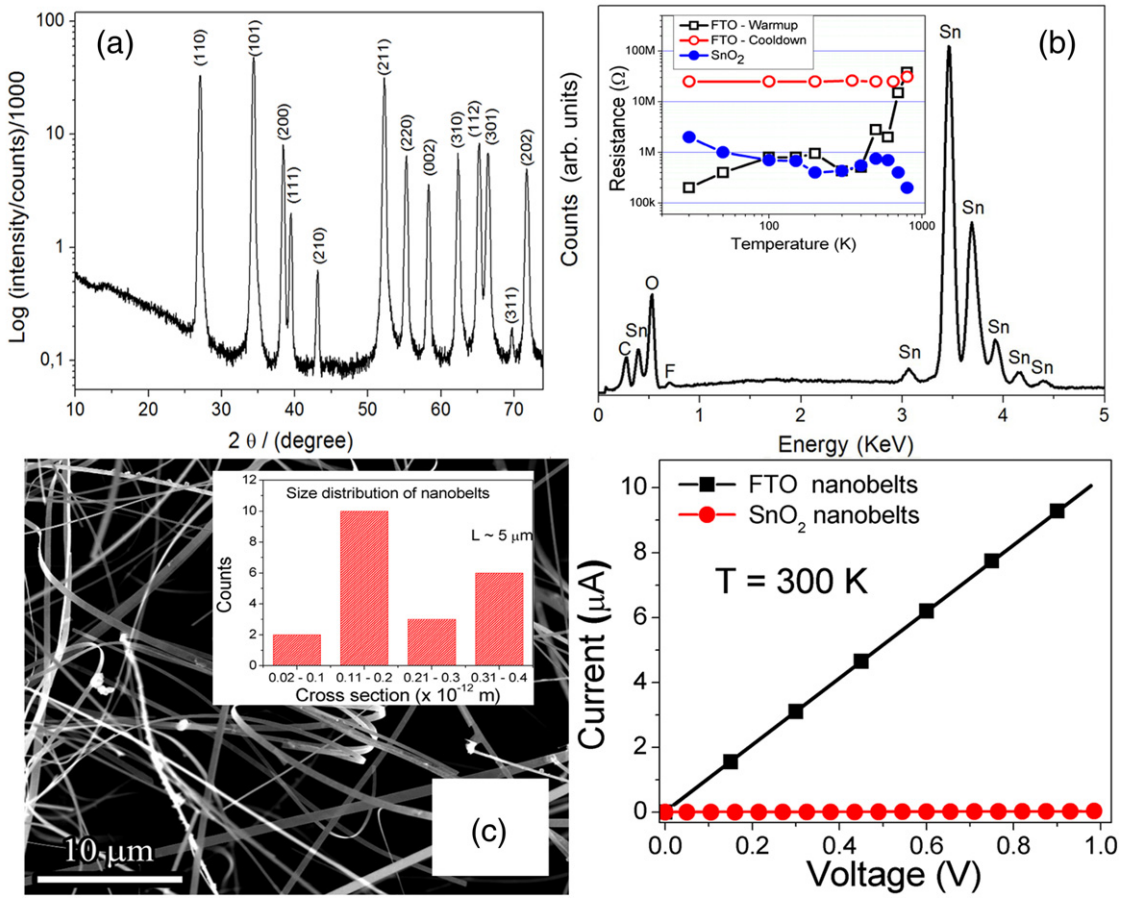

Figure 1. Structural and chemical composition characterization in FTO samples. (*a*) XRD diffraction pattern in log scale (PDF # 41-1445) of FTO obtained by carbothermal reduction process, (*b*) EDX spectrum used to quantify the chemical composition in samples. The inset shows the two probes resistance measurements performed in different temperatures for SnO_2 and FTO nanobelts. (*c*) depicts an SEM image of FTO nanobelts showing their morphology with length of several micrometres; in the inset is their distribution of sizes. In (*d*) is shown the current–voltage measurements comparing the performance of undoped SnO_2 and FTO nanobelts.

fluorine, energy-dispersive x-ray (EDX) spectroscopy analysis was performed.

As shown in figure 1(*b*), EDX spectrum reveals that the synthesized nanobelts are composed of Sn, O and F. The presence of F was clearly observed and the atomic ratio of F : Sn was estimated to be ∼4%; several nanobelts (up to 20) were studied using EDX and all the spectra have shown approximately the same atoms ratio. As further evidence of fluorine incorporation to the SnO_2 lattice, two probes resistance measurements were performed at different temperatures with the as-grown material (30 °C $< T <$ 900 °C): as the temperature increases, the samples show no resistance variation until 750 °C when it increases significantly, as viewed in the inset of figure 1(*b*). Resistance was also measured in the cooldown process and still remained at the higher observed value.

Considering that 750 °C is close enough to the synthesis temperature (600 °C) the resistance increase means that fluorine atoms were really incorporated to the SnO_2 lattice. Otherwise—for instance, fluorine atoms were physically adsorbed on the FTO nanobelts' surfaces—they would be evapourated at much lower temperatures. The microstructures were also characterized by SEM: the as-grown material presented long nanobelts as can be observed in the inset of figure 1(*c*) (and expected for the VS process). In this case the vapour deposition will occur preferentially in faces with high energy resulting in elongated structures [4, 30]. The statistical distribution of nanobelts' sizes is depicted in the inset of figure 1(*c*).

As a first characterization we conducted resistance measurements in a single FTO nanobelt device, and as expected, the resistance showed a semiconducting behaviour at all used temperatures. The measured current–voltage curves of both doped and undoped SnO_2 (used for comparison) samples are shown in figure 1(*d*). The resistance of the undoped SnO_2 nanobelt was observed to be very high (∼3 GΩ). After F doping, the resistance was calculated to be about 100 kΩ and current–voltage curves presented a linear behaviour.

The transport properties of the synthesized FTO nanobelts were studied by temperature-dependent electrical resistivity measurements and the relevant results are displayed in figure 2. The resistivity data revealed a monotonic decrease with increasing temperature, a typical behaviour observed in semiconductor systems [31]. The values of $\rho(T)$ at 10 and 300 K were found to be 106 mΩ cm and 12 mΩ cm, respectively. These values of $\rho(T)$ are very close to the literature and further indicate that FTO nanobelts are excellent candidates for practical applications as TCOs. In addition to

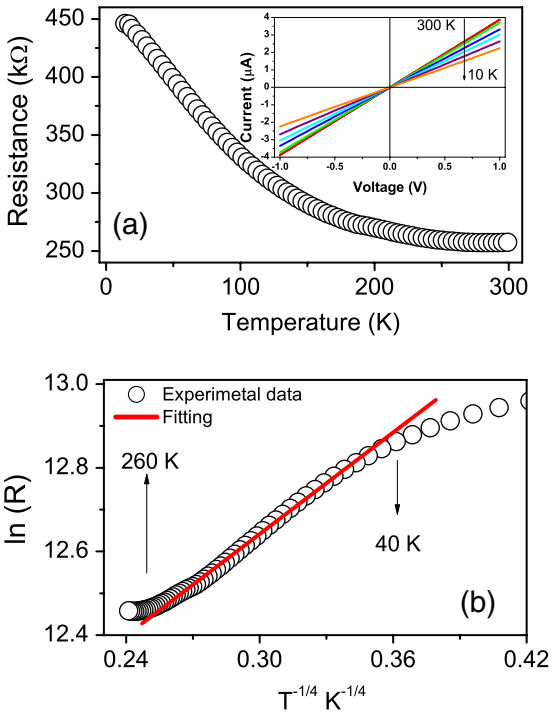

Figure 2. The resistance dependence on temperature for a single SnO_2 : F nanobelt device is depicted in panel (*a*). (*b*) shows the fitting of VRH conduction mechanism to the experimental data.

this, they are in good agreement with $\rho(T) \sim 4.3\,\mathrm{m\Omega\,cm}$ reported in FTO thin films [25], $\rho(300\,\mathrm{K}) \sim 1.3\,\mathrm{m\Omega\,cm}$ and $\sim 1\,\mathrm{m\Omega\,cm}$ for ITO and antimony doped tin oxide thin films, respectively [22, 25]. The ratio $[\rho(300\,\mathrm{K})/\rho(10\,\mathrm{K})]$ was found to be 0.11 for FTO nanobelts and it is essentially similar to that found in ATO thin films (0.1) [22].

Samples grown by a self-assembled method (VS mechanism in our case [29]) can exhibit metallic or semiconductor behaviour depending on the disorder originating from both growth process and doping [32]. The disorder in samples can lead the conduction of charges to present some localized character at low temperatures. From our experience [3–5] and from the literature, the VRH process of electric conduction can be more relevant when some disorder is present, and it is described by [34, 35]

$$\rho(T) = \rho_0 \exp\left[\left(\frac{T_0}{T}\right)^m\right], \qquad (1)$$

where $T_0 = 5.7\alpha^3/k_B N(E_F)$. Here, $N(E_F)$ is the DOS at the Fermi level and α^{-1} is the localization length and other constants have their usual meanings. This mechanism usually occurs in a temperature region where the energy is insufficient to excite the charge carriers through the Coulomb gap between two states. Since conduction takes place by hopping in a small region ($k_B T$) in the vicinity of the Fermi level where the DOS remains almost a constant ($m = 1/(d+1)$, where d is the system dimensionality) [35]. Thus, from temperature-dependent resistivity measurements we were able to study the conduction character in our samples. The inset of figure 2(*a*) shows current–voltage curves for different temperatures (10–300 K) revealing the ohmicity of the electric contacts for the whole range of temperatures. The $\rho \times T$ curve in figure 2(*a*) clearly exhibits a semiconducting character: decreasing of resistance with increasing temperature. It is interesting to note that a simple model based on the thermal activation law [$\rho(T) \sim \exp(\frac{\Delta E}{k_B T})$] or Efros VRH mechanism [$\rho(T) = \exp(\frac{T_{1/2}}{k_B T})^{1/2}$] [33] was unable to explain the observed behaviour because some physical parameters, such as localization length or excitation energy, invariably assume unreasonable values. The fitting of equation (1) to the experimental data revealed that the mechanism transport is mainly governed by the VRH process. The fitting of low dimensionality hopping laws ($d = 1$) and ($d = 2$) were also performed but were discarded due to the poor agreement between these mechanisms and the data. Through the fitting of equation (1) (figure 2(*b*)) to expected data, we obtained $T_0^{1/4} = 4.3\,K^{1/4}$.

Considering the energy states to be uniformly distributed (this assumption is reasonable for the spatial extension of the carrier wave function in our samples) we calculated the characteristic carrier localization length. The DOS for SnO_2 is estimated to be $N(E_F) \sim 10^{20}\,\mathrm{cm^{-3}\,eV^{-1}}$ from literature and as far we know this value is similar for both doped or undoped SnO_2 [22, 25, 36]. From the VRH fitting we obtained 4 nm for the localization length, which is in full agreement with the Bohr radius of SnO_2 (3.3 nm) and it is smaller than cross section of the nanobelt ($300 \times 30\,\mathrm{nm^2}$) thus evidencing the three-dimensional character of the transport [37]. From T_0 it was also possible to obtain the mean hopping distance, i.e. the distance an electron must hop for conduction. At 300 K the hopping distance was estimated to be [33]

$$\overline{R}_{hop} = \left(\frac{1}{\alpha}\right)\left(\frac{9}{8\pi\beta}\right)^{1/4}\left(\frac{T_0}{T}\right)^{1/4} = 5.2\,\mathrm{nm}. \qquad (2)$$

After these initial investigations on the conduction character of the samples, three terminal devices were built to obtain data on FTO performance as the active channel in a transistor device: from these measurements we were able to estimate the density and mobility of carriers which are essential for devices developing. Figure 3(*a*) shows a set of transistor characteristic curves (I_{DS}–V_{DS}) at different gate voltages (V_{Gate}). The gate effect is rather weak: this is probably caused by the large dimensions of the channel ($\sim 5\,\mu$m) associated with the unavoidable presence of disorder. Figure 3(*b*) depicts $I_{DS} - V_{Gate}$ curves of FTO nanobelt FET which exhibit an excellent conductance response to gate voltage: the FTO channel was fully turned off even at $V_{Gate} = -15$ V and the transconductance (figure 3(*b*)) exhibited the maximum value of 72.4 nS at $V_{Gate} = -20$ V ($V_{DS} = 1$ V). The device exhibited a good ON/OFF ratio of 10^4, in agreement with those found in the literature for SnO_2 based materials [12, 38, 39]. The electron mobility (μ) in FTO nanobelt FET was calculated by [12, 38, 39]

$$g_m = \frac{dI_{SD}}{dV_{Gate}} = \frac{\mu C}{L^2}, \qquad (3)$$

where μ is the carrier mobility, L is the length of the active nanobelt channel, g_m is the transconductance obtained through figure 3(*a*) and the capacitance C is given by [12, 38, 39]

$$C = \frac{2\pi\epsilon_0\epsilon_{SiO_2}L}{\cosh^{-1}\left(\frac{2h+d}{d}\right)}, \qquad (4)$$

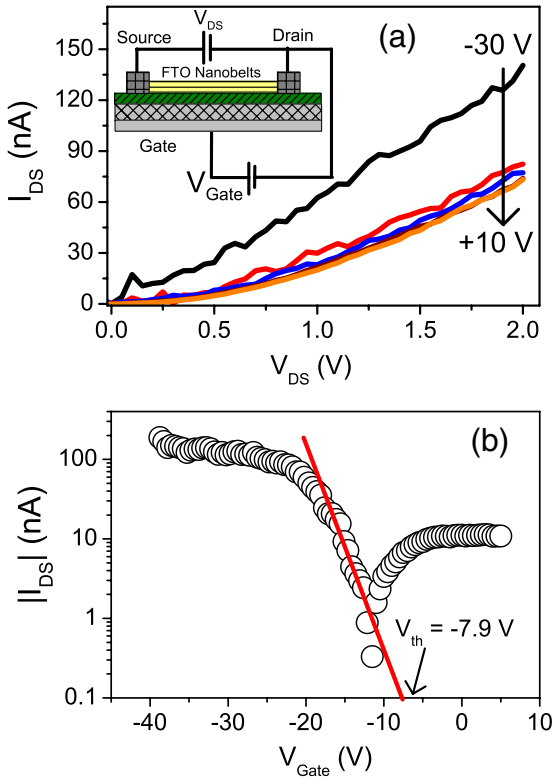

Figure 3. Transistor characteristics of back-gated FTO nanobelt FET devices on oxidized silicon substrates. (*a*) Family of drain to source current curves at different gate voltages is depicted from −30 to 10 V in 10 V steps (from top to bottom). (*b*) Drain to source current as a function of gate voltages at the linear region ($V_{DS} = 1$ V). The inset in (*a*) shows a sketch of the transistor device and the typical measuring circuit.

where $\epsilon_{SiO_2} = 3.9$ is the dielectric constant of the SiO_2 gate, $h = 1\,\mu$m is its thickness, and $d \simeq 30$ nm is the lateral size of the nanobelt. It should be noted that equation (4) evolves into the commonly used capacitance model $C_g = \frac{2\pi\epsilon_0\epsilon_{SiO_2}L}{\ln(\frac{4h}{d})}$ when $h \gg d$; we estimated a capacitance of 280 aF using the equation (4). Using this value and measuring the transconductance (g_m), the mobility of 48 cm^2 V^{-1} s^{-1} was obtained. From threshold voltage figure 3, $V_{th} = -7.9$ V, we estimated the carrier concentration, n_e, using [39, 40]

$$n_e = \frac{V_{th}C}{q\pi\left(\frac{d}{2}\right)^2 L}, \qquad (5)$$

and we found $n_e = 2 \times 10^{18}$ cm^{-3}. Taking into account the VRH mechanism, the carriers participating in the hopping process are those which have an energy such that $E - E_F \sim k_BT$ [34] and then, the carrier density can be written as $n_e \sim k_BTN(E_F)$ [34]. Using this relationship, we calculated the DOSs of FTO samples to be $\sim 10^{20}$ cm^{-3} which is in excellent agreement with the value used for the hopping distance calculation described above. Finally, using the density of carriers and considering Coulomb interactions between fluorine donors, we estimated the fluorine–fluorine distance to ∼5.0 nm which is also in agreement with the $\overline{R}_{hop}$ [33]. This means that hopping distance is nearly equal to the average distance between two fluorine atoms [41], thus confirming that fluorine atoms were incorporated into the SnO_2 lattice.

4. Conclusion

Briefly, we have synthesized fluorine doped SnO_2 and investigated their transport properties. From single nanobelt devices we observed the variable range hopping as the dominant mechanism in a large range of temperature (40–260 K). These data provide us with an estimate of the localization length (4 nm) and hopping distance (5.2 nm at 300 K) showing that the studied FTO nanobelts exhibit a three-dimensional character for carrier transport. The electrical data from transistor characterization revealed a mobility of 48 cm^2 V^{-1} s^{-1} and carrier density of 2×10^{18} cm^{-3}. Taking into account the variable range hopping mechanism and these data we found directly the characteristic density of states at Fermi level in our samples.

Acknowledgments

This work was financed by the Brazilian Agencies under grants 141488/2010-7 and 302640/2010-0 (CNPq) and grant 2011/10171-1 São Paulo Research Foundation (FAPESP).

References

[1] Ajayan P M and Redlich P 1997 *J. Microsc.* **185** 275
[2] Hoel, C A, Mason, T O, Gaillard, J F and Poeppelmeier K R 2010 *Chem. Mater.* **22** 3569
[3] Amorim C A, Berengue O M, Kamimura H, Leite E R and Chiquito A J 2011 *J. Phys.: Condens. Matter* **23** 205803
[4] Lanfredi A J, Geraldes R R, Berengue O M, Leite E R and Chiquito A J 2009 *J. Appl. Phys.* **105** 023708
[5] Chiquito A Lanfredi R F O, Pozzi L P and Leite E R 2007 *Nano Lett.* **7** 1439
[6] Lupan O, Chowa L, Pauporté Th, Ono L K, Roldan Cuenya B and Chai G 2012 *Sensors Actuators* B **173** 772
[7] Changhyun J, Hyunsu K, Sunghoon P, Hyoun W K, Sangmin L and Chongmu L 2012 *Ceram. Int.* **38** 6585
[8] Changhyun J, Chanseok H, Sunghoon P and Chongmu L 2010 *Thin Solid Films* **519** 1351
[9] Lupan O, Chowa L, Chaic G, Schultea A, Parka S and Heinrich H 2009 *Mater. Sci. Eng.* B **157** 101
[10] Fan Z, Wang D, Chang P C, Tseng W Y and Lu J G 2004 *Appl. Phys. Lett.* **85** 5923
[11] Zhang D, Liu Z, LiC, Tang T, Liu X, Han S, Bo L and Zhou C 2004 *Nano Lett.* **4** 1919
[12] Dattoli E N, Wan Q, Guo W, Chen Y, Pan X and Lu W 2007 *Nano Lett.* **7** 2463
[13] Sanghyun J, Antonio F, Yi X, Jun L, Fumiaki I, Peide Y, Chongwu Z, Tobin J M and David B J 2007 *Nature Nanotechnol.* **2** 378
[14] Kovtyukhova N I and Mallouk T E 2002 *Chem.—Eur. J.* **8** 4354
[15] Ma Y J, Zhou F and Zhang Z 2004 *Solid State Commun.* **130** 313
[16] Arnold M S, Avouris P, Pan Z W and Wang Z L 2003 *J. Phys. Chem.* B **107** 659
[17] Liu Z, Zhang D, Han S, Li C, Tang T, Jin W, Liu X, Lie B and Zhou C 2003 *Adv. Mater.* **15** 1754
[18] Wan Q, Dattoli E N and Lu W 2007 *Appl. Phys. Lett.* **90** 222107
[19] Kim K H, Lee S W, Shin D W and Park C G 1994 *J. Am. Ceram. Soc.* **77** 915

[20] Chopra K L, Mayor S and Pandya D K 1983 *Thin Solid Films* **102** 1
[21] Minami T, Takata S, Sato H and Sonohara H 1995 *J. Vac. Sci. Technol.* A **13** 1095
[22] Giraldi T R, Escote M T, Maciel A P, Longo E, Leite E R and Varela J A 2006 *Thin Solid Films* **515** 2678
[23] Sun J, Lu A, Wang L, Hu Y and Wan Q 2009 *Nanotechnology* **20** 335204
[24] Shanthi S, Subramanian C and Ramasamy P 1999 *Mater. Sci. Eng.* B **57** 127
[25] Aouaj M A, Diaz R, Belayachi A, Rueda F and Abd-Lefdil M 2009 *Mater. Res. Bull.* **44** 1458
[26] Bilgin V, Akyuz I, Ketenci E, Kose S and Atay F 2010 *Appl. Surf. Sci.* **256** 6586
[27] Wan Q and Wang T H 2005 *Chem. Commun.* **30** 3841
[28] Purushothaman K K, Dhanashankar M and Muralidharan G 2009 *Curr. Appl. Phys.* **9** 67
[29] Wagner R S and Ellis W C 1964 *Appl. Phys. Lett.* **4** 89
[30] Berengue O M, Simon R A, Chiquito A J, Dalmaschio C J, Leite E R, Guerreiro H A and Guimarães F E G 2010 *J. Appl. Phys.* **107** 033717
[31] Sze S M 1981 *Physics of Semiconductor Devices* (New York: Wiley)
[32] Russo B and Cao G Z 2008 *Appl. Phys.* A **90** 311
[33] Sato T, Ohashi K, Sugai H, Sumi T, Haruna K, Maeta H, Matsumoto N and Otsuka H 2000 *Phys. Rev.* B **61** 12970
[34] Mott N F 1990 *Metal–Insulator Transitions* (London: Taylor and Francis)
[35] Alexander M N and Holcomb D F 1968 *Rev. Mod. Phys.* **40** 815
[36] Hongwei L, Cheng S, Junpeng L, Zhengi M, Lim K Y, Nripan M, Subodh G M, Tang S H, Zhang X and Sow C H 2012 *RSC Adv.* **2** 9590
[37] Wu H C, Huang Y C, Ding I K, Chen C C, Yang Y H, Tsai C C, Chen C D and Chen Y T 2011 *Adv. Funct. Mater.* **21** 474
[38] Sun J, Tang Q, Lu A, Jiang X and Wan Q 2009 *Nanotechnology* **20** 255202
[39] Cheng Y, Yang R, Zheng J P, Wang Z L and Xiong P 2012 *Mater. Chem. Phys.* **137** 372
[40] Goldberger J, Sirbuly D J, Law M and Yang P 2005 *J. Phys. Chem.* B **109** 9
[41] Schirmacher W 1990 *Phys. Rev.* B **41** 246